Journal of Medicinal Chemistry

pubs.acs.org/jmc

Article

Discovery of the Bruton's Tyrosine Kinase Inhibitor Clinical Candidate TAK-020 (*S*)-5-(1-((1-Acryloylpyrrolidin-3-yl)oxy)isoquinolin-3-yl)-2,4-dihydro-3*H*-1,2,4-triazol-3-one, by Fragment-Based Drug Design

Mark Sabat,* Douglas R Dougan, Beverly Knight, J. David Lawson, Nicholas Scorah, Christopher R Smith, Ewan R Taylor, Phong Vu, Corey Wyrick, Haixia Wang, Deepika Balakrishna, Mark Hixon, Loui Madakamutil, and Donavon McConn

Cite This: https://doi.org/10.1021/acs.jmedchem.1c01026

Read Online

ACCESS | Metrics & More | Article Recommendations | Supporting Information

ABSTRACT: This publication details the successful use of FBDD (fragment-based drug discovery) principles in the invention of a novel covalent Bruton's tyrosine kinase inhibitor, which ultimately became the Takeda Pharmaceuticals clinical candidate TAK-020. Described herein are the discovery of the fragment 5-phenyl-2,4-dihydro-3*H*-1,2,4-triazol-3-one, the subsequent optimization of this hit molecule to the candidate, and synthesis and performance in pharmacodynamic and efficacy models along with direct biophysical comparison of TAK-020 with other clinical-level assets and the marketed drug Ibrutinib.

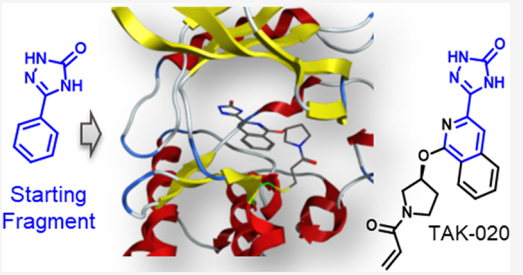

INTRODUCTION

Rheumatoid arthritis (RA) is a chronic incurable autoimmune disease characterized by swelling and erosion of the joints in early stages.[1a] Joint deformity and loss of function are progressive if untreated, leading to disability and potential organ involvement with reduction in life quality and lifespan. RA prevalence has been estimated at up to 1% of the adult population in the developed world.[1b] Current treatment is focused on early intervention and aggressive treatment with small-molecule and targeted biologic disease-modifying anti-rheumatic drugs (DMARDS) to achieve low disease activity and ideally remission.[1c] Patient outcomes have turned more favorable with current treatment regimens; however, the presence of many nonresponders highlights the need for novel treatments.

Small-molecule DMARDS have evolved from broad anti-inflammatory agents to more recent targeted approaches involving the Janus kinase (Jak) inhibitors, tofacitinib, and baricitinib.[2] These first kinase inhibitors approved for the treatment of RA demonstrate comparable American College of Rheumatology (ACR) scores to multiple biologics and underscore the new small-molecule opportunities available for effective disease intervention.

Btk is a member of the Tec family of nonreceptor tyrosine kinases and is expressed in B cells,[3] mast cells,[4] monocytes/macrophages,[4b,5] neutrophils,[6] dendritic cells,[7] erythroid cells,[4b,8] platelets,[9] hematopoietic stem cells, and multipotent progenitors.[10] Examination of patients with the inherited immunodeficiency disease X-linked agammaglobulinemia (XLA) revealed that loss of function mutations in the Btk gene prevents the development of B cells, causing an almost complete depletion of B cells and circulating immunoglobulins.[3] These findings indicate that Btk inhibition could be an attractive approach for the treatment of autoimmune diseases such as RA.

Various groups have published reports on small-molecule Btk inhibitors with demonstrated efficacy in rodent models of collagen-induced arthritis (CIA) and systemic lupus erythematosus (SLE)[11] providing additional support for the role of Btk in autoimmune disease. Ibrutinib **1**[12a] and Acalabrutinib **2**[12b] (Figure 1) are currently marketed irreversible covalent inhibitors of Btk for the treatment of mantle cell lymphoma and chronic lymphocytic leukemia.[12c] When we entered the search for a best-in-class Btk inhibitor to treat RA and related autoimmune conditions, both noncovalent[13b] and covalent approaches were explored. To maximize our chances for successfully delivering a safe and selective covalent Btk inhibitor in a nononcologic indication, the Takeda team

Received: June 8, 2021

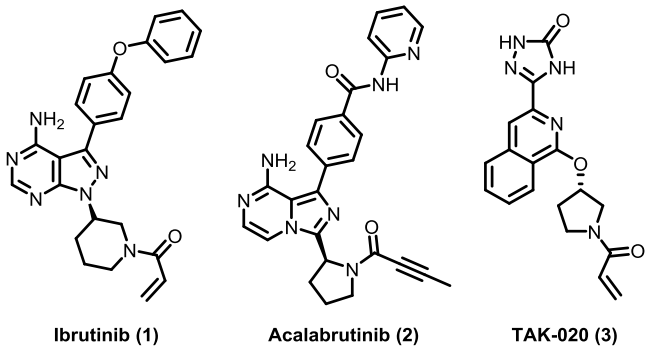

Figure 1. Covalent Btk inhibitors.

utilized a fragment-based approach as we described before in a conventional noncovalent campaign on this target.[13b]

RESULTS AND DISCUSSION

Identification and Characterization of Fragment Leads. Takeda has focused on fragment-based drug design (FBDD) as a methodology for lead compound identification. A key driver for using FBDD was the anticipated reduced cycle time to identify novel chemical leads compared to high-throughput screening (HTS). FBDD starts with a chemical library of low-molecular-weight (MW) compounds (typical MW of ∼150−300 Da) and selects through screening entities that form high-quality ligand−protein interactions and then subsequently grows them in the most ligand-efficient way.[14a] The FBDD process guided by tracking ligand efficiency (LE)[14b] and ligand lipophilicity efficiency (LLE)[14c] metrics during the optimization favors the discovery of drug molecules with better physical properties, high target potency, improved selectivity, and ultimately lower human dose and clinical attrition.[14d]

A library of 11,098 compounds ($11 \leq$ HA ≤ 19; $-1.0 \leq$ clogP ≤ 3) was screened biochemically at 200 μM using a Caliper mobility shift assay (Caliper Life Sciences, Hopkinton, Massachusetts). A 4.6% hit rate was observed by defining a hit as >40% inhibition at 200 μM. Hits were selected for crystallography based on a subjective assessment of fragment structure novelty, LE, and after confirmation of binding by saturated transfer difference ^{1}H NMR. A total of 20 X-ray crystallographic coliganded structures were solved for fragments across a range of potencies (Btk pIC_{50} of 3.3−5.5) and ligand efficiencies (LE of 0.53−0.38) (Table 1).[13a] The most potent and ligand-efficient fragment, fragment **4**, was previously optimized and yielded a series of potent and selective reversible Btk inhibitors previously reported by Smith and coworkers.[13b] This publication will focus on the triazolone fragment hits, fragments **5** and **6**, and their elaboration into the clinical candidate TAK-020 (**3**; Figure 1). The triazolone hits were selected for further investigation on account of ligand efficiencies, strong electrostatic interactions with protein hinge residues, and the novel nature of this functional group in kinase inhibitor discovery with no previous examples reported.

Fragment Growing. Examining a cocrystal structure of fragment **5** in Btk (PDB code 7N5O) reveals a 3-substituted 1,2,4-triazolone, which interacts with the gatekeeper Thr-474 via its carbonyl group (Figure 2A). This interaction should confer greater kinome selectivity as only ∼21% of typical human kinases possess a threonine or serine gatekeeper.[15] This carbonyl moiety also makes favorable interactions with the

Table 1. Biochemical and Biophysical Characterization of Fragment Hits 4−6

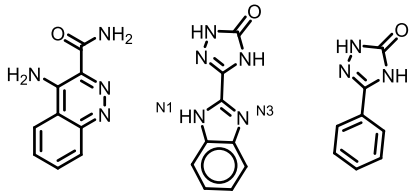

cmpd no.	HA[a]	clogP[b]	Btk pIC_{50}[c]	LE[d]
4	14	0.2	5.5	0.53
5	15	1.0	5.0	0.45
6	12	2.4	3.3	0.38

[a]HA = heavy atoms. [b]Calculated logarithm of the octanol/water partition coefficient using JChem (ChemAxon) version 5.11.2. [c]Enzyme IC_{50} was determined in duplicate as described in the Supporting Information. [d]LE = $(1.36 \times pIC_{50})$/HA.

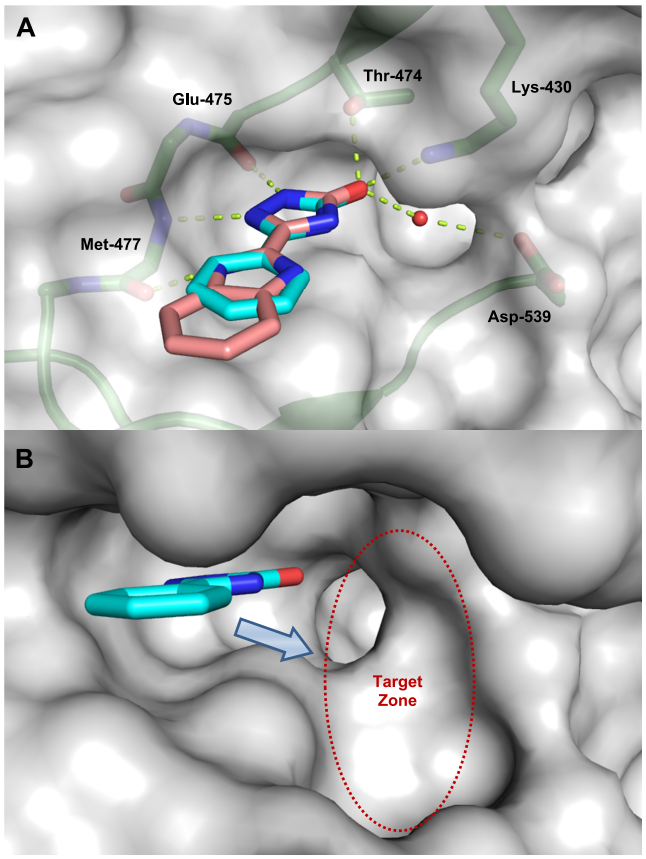

Figure 2. (A) X-ray crystal structures of fragments **5** (salmon; 7N5O) and **6** (cyan; 7N5R) in the ATP binding site of Btk. The P-loop region has been removed for clarity. (B) Target zone and vectors from fragment **6**.

canonical salt bridge via a H-bond with Lys-430 and a water-mediated H-bond with Asp-539 although it should be noted that the density is weak for Lys-430, so it likely exists in multiple conformations. Fragment **5** also interacts with hinge residues Glu-475 (via the triazolone) and Met-477 (via both the triazolone and the benzimdazole moieties). This series of electrostatic interactions emanating from the triazolone group anchors the fragment but offers no direct vectors to grow

https://doi.org/10.1021/acs.jmedchem.1c01026
J. Med. Chem. XXXX, XXX, XXX−XXX

Table 2. Heavy-Atom Count, clogP, Btk Enzyme Inhibition, LE, LLE, and Cellular Potency for Compounds 7−24 and TAK-020 (3)

Cmpd#	Structure	HA[a]	clogP[b]	Btk pIC50[c]	LE[d]	LLE[e]	pBtk pEC_{50}[f]
7		12	-0.23	3.5	0.40	3.8	-
8		12	0.08	3.9	0.44	3.8	-
9		14	0.9	4.5	0.44	3.6	-
10		14	0.51	4.0	0.39	3.5	-
11		15	1.26	5.2	0.47	3.9	-
12	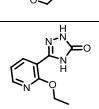	15	0.87	< 4.0	-	-	-
13	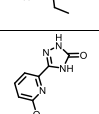	17	2.14	5.8	0.47	3.7	-
14	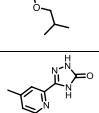	17	2.19	6.6	0.53	4.4	-
15		16	1.45	5.3	0.45	3.9	-
16		18	1.89	6.4	0.48	4.5	-
17		18	1.89	5.5	0.41	3.6	-
18	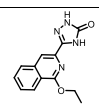	19	2.25	7.3	0.52	5.0	-
19		19	1.88	7.0	0.50	5.2	6.1
20		20	2.29	7.7	0.53	5.4	6.8
21	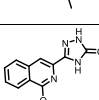	20	2.66	8.0	0.55	5.4	7.0
22	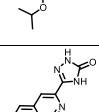	20	2.77	7.6	0.52	4.9	6.4
23	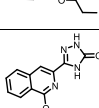	25	1.08	7.5	0.41	6.4	-
24		26	1.84	7.5	0.41	6.4	6.3
TAK-020 (3)		26	1.84	>8.7	0.46	6.7	8.9

[a]HA = heavy atoms. [b]Calculated logarithm of the octanol/water partition coefficient using JChem version 5.11.2. [c]Enzyme IC_{50} was determined in duplicate as described in the Supporting Information. [d]LE = (1.36 × pIC_{50})/HA. [e]LLE = pIC_{50} − clogP. [f]Cellular Btk inhibition was measured using the PhosY223 Btk HTRF assay from Cisbio in a RAJI cell line S32.

deeper into the Btk protein. The 2-benzimidazole ring portion of triazolone **5** appeared to offer vectors for growth. However, the most desirable location to begin growth was N3. Substitution at N3 was not directly possible without loss of the hinge N1-H interaction with Met-477. Therefore, for synthetic simplicity, we elected to work initially with fragment **6** (PDB code 7N5R). This compound was also cocrystalized with Btk and maintained all the triazolone ring positive interactions and replaced the H-bond between the Met-477 backbone carbonyl and the benzimidazole proton with a nonclassical (pseudo) H-bond from the hydrogen at the 2-position of the phenyl ring. More importantly, fragment **6** provided direct vectors deeper into the binding pocket. Starting point **6** initially appeared suboptimal to the team due to its greater lipophilicity, lower LE, and low binding affinity. However, the reduced HA count, hydrogen bond donor (HBD) count, and easy access to a wide variety of starting materials allowed for quick initial exploration of the binding site that was ultimately fruitful.

Initial exploration of compound **6** focused on determining the best position to introduce an sp^2 nitrogen atom to mimic the sp^2 N3 hydrogen bond acceptor (HBA) found in fragment **5**. The two possible points of elaboration are exemplified in analogs **7** and **8**, with compound **8** appearing to be more potent. As we wanted to grow from the position adjacent to the pyridyl nitrogen, a methoxy group was introduced in analogs **9** and **10** to see if an alkoxyl group would be tolerated. While compound **10** was approximately equipotent to parent **8**, compound **9** showed a 10-fold better potency and improved LE vs parent **7**. Incremental growth with ethoxy vs methoxy (analogs **11** and **12**) reaffirms the trend of the C6 vector being superior for alkoxy substitution. Compound **11** showed a further improved LE = 0.47 and binding potency pIC_{50} = 5.2 as contrasted against **9** (LE = 0.44; pIC_{50} = 4.5). A further addition of two heavy atoms (analogs **13** and **14**) again indicated growth at C6 to be clearly favored with an increase of LE and LLE being achieved for both analogs. Compound **14** in fact showed an impressive pIC_{50} of 6.6. This boost in activity

https://doi.org/10.1021/acs.jmedchem.1c01026
J. Med. Chem. XXXX, XXX, XXX−XXX

and efficiency metrics suggested that more could be gained by growing off the 4-position of the pyridine ring. To facilitate synthetic tractability, inspired by the initial bicyclic fragment hit **5** and in agreement with modeling, the pyridine ring was morphed to an isoquinoline to give **15** and then incrementally substituted to the related **16**. Although compound **16** was slightly less ligand-efficient and potent as compared to **14**, the LLE was maintained, and the change was accepted for synthetic ease. Analog **17** (structural isomer of **16**) confirms the earlier ring substitution preference observed with the pyridine analogs (compare **9** vs **10** to **16** vs **17**). Progressing from **16** with the addition of one heavy atom gives **18** (LE = 0.52, LLE = 5.0, and pIC_{50} = 7.3). With the achievement of this level of Btk binding potency ~ pIC_{50} = 7, we began to test our compounds in a secondary low-throughput cellular assay (details in footnotes of Table 2 and the SI). This assay measured phosphorylated Btk (pBTK) in RAJI cells stimulated with anti-IgM. With compound **18** showing a substantial increase in efficiency and potency, we next briefly explored alternative C6 linkers using a nitrogen atom (see **19** and **20**) for their effect on activity. These ethylamine- and isopropyl amine-substituted analogs maintained good metrics and activity and good cellular pBTK inhibition (**19** pEC_{50} = 6.1, **20** pEC_{50} = 6.8), with a modest increase in LLE at the cost of an additional hydrogen bond donor. As the triazolone starting point contained 2 HBD and there was no advantage in the switch from −O−alkyl to −NH−alkyl, we returned to the oxygen linker for future analogs to reduce any concerns related to a higher desolvation penalty for the additional −NH and its possible effect on membrane permeability. With the synthesis of *o*-isopropyl and *o*-propyl analogs **21** and **22**, we were pleased to see increased activity for both with a 10-fold increase in potency and improved efficiency for **21** (pIC_{50} = 8.0; LE = 0.55; LLE = 5.4). This compared favorably with the earlier analog **14** suggesting the choice to add a second ring justified. To better understand the SAR of the *o*-alkyl series and guide the design of additional compounds, an X-ray cocrystal structure of *o*-ethyl analog **18** was obtained (Figure 3).

Examination of the X-ray cocrystal structure of compound **18** (PDB code 7N5X) (Figure 3) combined with modeling of compounds **21** and **22** revealed the *o*-alkyl groups partially filling the pocket adjacent to the triazolone-isoquinoline scaffold with direct van der Waals interactions with the P-loop. In addition, analysis indicated that the addition of a covalent warhead, such as acrylamide, had the potential to covalently modify Cys-481. Modeling various saturated rings that would encompass the ethyl substituent on **18** and direct toward the Cys-481 appeared to favor a pyrrolidine ring. We therefore constructed analog **23** and were pleased with the increase in LLE with only a modest decrease in potency. Molecular modeling and short trajectory molecular dynamics simulations suggested that installation of the acrylamide electrophile on the pyrrolidine ring would position this group in a reactive geometry relative to the Cys-481 sulfur. We envisaged that the *S* enantiomer would be preferred from models but made both (*R*)-**24** and (*S*)-**3**. The superior potency of compound **3** confirmed our predictions. We turned to X-ray cocrystallography to substantiate the covalent modification of Cys-481in Btk (Figure 4) by **3** (PDB code 7N5Y). Analysis of the costructure of **3** in Btk revealed the triazolone and isoquinoline rings keeping the same interactions as seen in previous structures with the exception of the direct H-bond to Lys-430 being replaced with a water-mediated H-bond. This was likely due to the natural mobility of the lysine side chain noted earlier and variability between structures, not due to a difference caused by the ligand. One edge of the pyrrolidine ring overlaid the ethyl moiety of **18** further validating our modeling efforts. The covalent link between the terminal acrylamide (now ethyl) carbon and the Cys-481 sulfur can clearly be seen overlaid with residual density for a small, unreacted population of proteins and ligands.

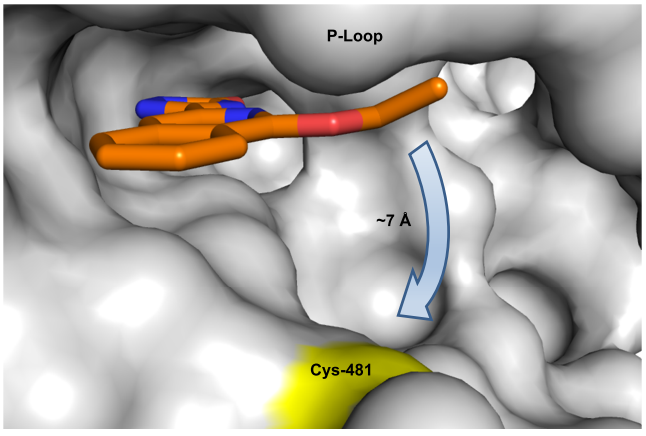

Figure 3. X-ray crystal structure of compound **18** (PDB code 7N5X) bound in the ATP binding site of Btk. The arrow highlights the vector toward Cys-481.

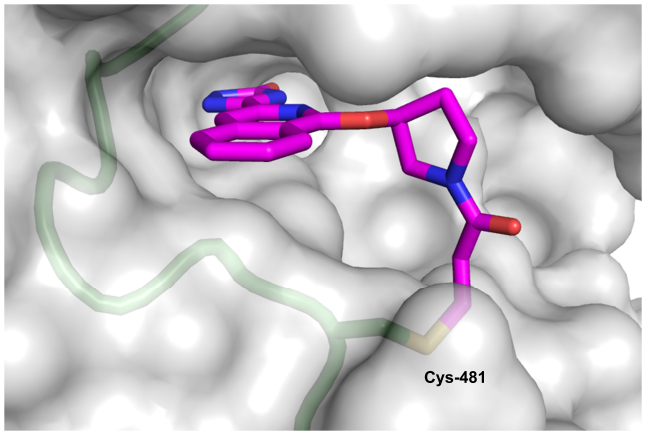

Figure 4. X-ray crystal structure of compound **3** (TAK-020; PDB code 7N5Y) covalently bound to Cys-481 in the ATP binding site of Btk.

A concern of utilizing covalent drugs is the nonselective modification of physiological proteins. This can lead to unwanted idiosyncratic toxicity and hapten adduct formation with unwanted autoimmune activation or simply lead to unproductive degradation of drug species.[16] We next evaluated the intrinsic reactivity of **3** (nonenzymatic) and the potential bioactivation of this material. Compound **3** was incubated in buffer with and without 10 mM GSH as well as incubated in HLM (human liver microsomes, with and without GSH) (details of the experiment and data in the SI). Compound **3** was found to be stable in buffer for 2 h at 37 °C but appeared to have a small intrinsic reactivity as 75% remained after 2 h incubation with GSH in buffer. No significant bioactivation was observed, and we then looked at the broad kinome

https://doi.org/10.1021/acs.jmedchem.1c01026
J. Med. Chem. XXXX, XXX, XXX−XXX

selectivity and reactivity within a subset of kinases that contain reactive functionalities.

The closely related protein kinase Lck (lymphocyte-specific protein tyrosine kinase) causes T-cell activation;[17] hence, competitors have focused on achieving selectivity for Btk over Lck. Compound **3** demonstrated modest inhibitory activity against Lck (pIC_{50} = 6.0) and Src (pIC_{50} = 6.2), two structurally similar Src family kinases. We deemed this level of off-target activity acceptable. Further kinome selectivity profiling by determining % inhibition at 0.3, 1, and 3 μM of 303 kinases was conducted, and $ApIC_{50}$ (apparent IC_{50}) was calculated. Follow-up IC_{50} data was generated for the 10 kinases that inhibited >75% at 1 μM, and both are described in the Supporting Information (Tables S1 and S2). Of the 10 kinases rescreened in the follow-up only 7, (Jak3(h) = 42 nM; Blk(h) = 1.9 nM; BMX(h) = 1.1 nM; TXK(h) = 2.2 nM; EGFR(h) = 17.3 nM; ITK(h) = 99 nM; HER4 = 2.7 nM) showed an activity below 100 nM. Of these except for Jak3, all are members of the Tec and Src family kinases, which contain a cysteine residue that could potentially react with compound **3**. The data for these specific kinases was examined in terms of binding kinetics to better understand selectivity within this subset of kinases (the full data set is in SI Table S3). The team felt that the selectivity displayed by compound **3**, its rapid covalent interception of the target in blood, and the extremely low circulating concentration in vivo (discussed later in the publication) warranted further advancement of the compound.

Chemistry. The triazolone derivatives **3**–**24** described herein were prepared by two general methodologies as illustrated in Scheme 1.[18] Starting with an appropriately

Scheme 1. General Procedures for Synthesis of Compounds 3–24[a]

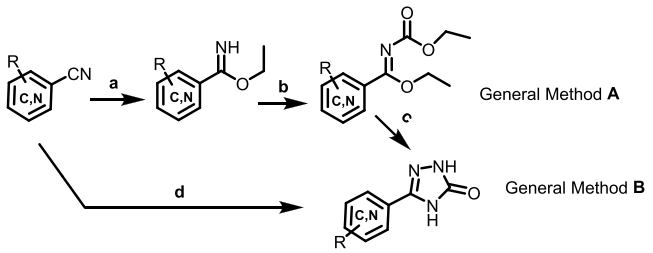

[a]Reagents and conditions: (a) (i) HCl(g), EtOH/DCM, 0 °C, 1 h then RT overnight, (ii) KOH, H_2O; (b) (i) ethyl chloroformate, trimethylpyridine, hexanes, RT, (ii) reflux, overnight; (c) hydrazine hydrate, CCl_4, reflux, 2 h; (d) ethyl hydrazinecarboxylate microwave, 165 °C, 5 h.

elaborated nitrile, the corresponding ethoxyimidate can be generated in EtOH under HCl(g). This material is then trapped with ethyl chloroformate. Treatment of this reactive intermediate with hydrazine hydrate at reflux in CCl_4 affords the desired triazolones. An alternative approach involved treating the starting nitrile with ethyl hydrazinecarboxylate neat under microwave heating.[18b] Although the single-step transformation was the most attractive, prolonged heating was often necessary, and yields were typically low. However, for quick exploration of analogs and SAR studies, it proved to be expeditious.

More complex bicyclic systems such as compound **3** incorporating electrophilic acrylamides required a modified procedure (Scheme 2). Treatment of the commercially available 1,3-dichloroisoquinoline (**I**) with the anion of (*S*)-*tert*-butyl 3-hydroxypyrrolidine-1-carboxylate affords **II**. For analogs such as **19** and **20**, the corresponding alkyl amines could be used directly in *n*-BuOH under microwave heating for addition to **I**. Conversion of the remaining Cl atoms to a nitrile using palladium-catalyzed cyanation gives **III**, which then can be further elaborated using the methods in Scheme 1. Specifically, to access compound **3**, general method B (Scheme 1) was used with the ethyl hydrazinecarboxylate being added to DBU/NMP at 170 °C, ON to make intermediate **IV**, which was deprotected with 4 N HCl, and the resulting amine was then treated with acryloyl chloride to give the final product.

Scheme 2. General Procedures for Synthesis of TAK-020 and Similar Analogs[a]

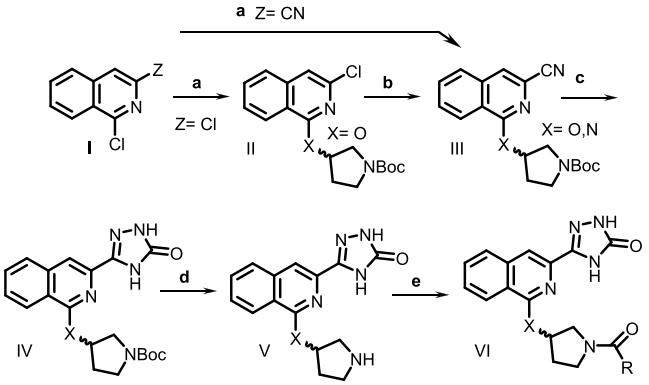

[a]Reagents and conditions: (a) for X = O, (i) (*S*)-*tert*-butyl 3-hydroxypyrrolidine-1-carboxylate, NaH NMP, 0 °C, 5 min, (ii) 1,3-dichloroisoquinoline, 5 min then 135 °C, 30 min microwave or (ii). For X = N alkylamine, *n*-BuOH, 180 °C 60 min microwave, (b) $ZnCN_2$, $Pd(PPh_3)_4$, trimethylpyridine, hexanes, 160 °C, 20 min microwave; (c) ethyl hydrazinecarboxylate, DBU/NMP, 170 °C, ON; (d) (i) 4 M HCl in dioxane, RT; (e) 2,6-dimethylpyridine, DCM, 0 °C, (ii) acryloyl chloride, 15 min, warmed to RT over 90 min.

Physicochemical Properties and ADMET Analysis of Compound 3. Thermodynamic solubility of **3** was examined in Japanese Pharmacopoeia Dissolution Test Fluid No. 1 (pH 1.2 (JP1)), Japanese Pharmacopoeia Dissolution Test Fluid No. 2 (pH 6.8 (JP2)), and in glycochenodeoxycholate containing biorelevant media GCDC (pH 6.8).[19] The solubility at acidic and neutral conditions in JP1 and JP2 fluids was <0.1 μg/mL and in GCDC was 6.8 μg/mL. Membrane permeability of **3** was measured in an LLC-PK1-MDR1[20] cell line determining Papp (A–B) (nm s^{-1}) = 18.9 and the efflux ratio (ER) = 10.8 (avg. of n = 4). In vitro clearance was assessed in liver hepatocytes across multiple species and reported as extraction ratios (E_h) showing low E_h in humans and rats to moderate E_h in monkeys, dogs, and mice (Table 3). Rat and human plasma protein binding (PPB) was determined to be ~90% for both species. Rat and dog in vivo clearance was near hepatic blood flow resulting in an apparent IV/IVE (in vitro–in vivo extrapolation) disconnection. These data suggest that additional routes of elimination may be in effect in vivo that are not captured in vitro.

Biophysical Comparison of Compound 3. Modern covalent drugs have been termed TCIs (targeted covalent inhibitors),[16d] a designation that encompasses the two-step process of time-dependent target inhibition. Initially, the drug (I) forms a reversible complex (EI) with its enzyme target. This is followed by a reaction between its weakly electrophilic warhead and a weak nucleophilic residue from the enzyme to

https://doi.org/10.1021/acs.jmedchem.1c01026
J. Med. Chem. XXXX, XXX, XXX–XXX

Table 3. In Vitro ADME and Pharmacokinetic Profile of 3[g]

species	liver hepatocyte (E_h)[a]	plasma protein binding (PPB)[b]	IV CL (mL min^{-1} kg^{-1})	in vivo (E_h)[e]	IV $t_{1/2}$ (h)	%F[f]
mouse	0.62					
rat	0.31	90.2	83.2[c]	>0.9	0.7	6.0
dog[d]	0.48		28.5[d]	0.81	3	6.5, 16.5
monkey	0.37					
human	0.21	88.7				

[a]E_h extraction ratio. [b]Rapid equilibrium dialysis method. [c]Male Sprague–Dawley rats (n = 2) dosed with 0.6 mg kg^{-1} IV (20% β-cyclodextrin in 0.05 M methanesufonic acid, pH 3) and n = 3 rats dosed with 4.7 mg kg^{-1} PO (0.5% methylcellulose suspension). [d]Male Beagle dogs (n = 4) dosed with 1 mg kg^{-1} IV (10% Captisol; clear solution) and n = 4 dogs per PO dose group dosed with 3.8 and 30 mg kg^{-1} PO (20% Captisol; clear solution). [e]In vivo E_h extraction ratio = IV clearance/liver blood flow, where liver blood flow in rat = 70 mL min^{-1} kg^{-1} and dog = 35 mL min^{-1} kg^{-1}. [f]$F = 100 \times \frac{AUC_{PO}}{AUC_{IV}} \times \frac{Dose_{IV}}{Dose_{PO}}$. [g]See the Supporting Information for more details.

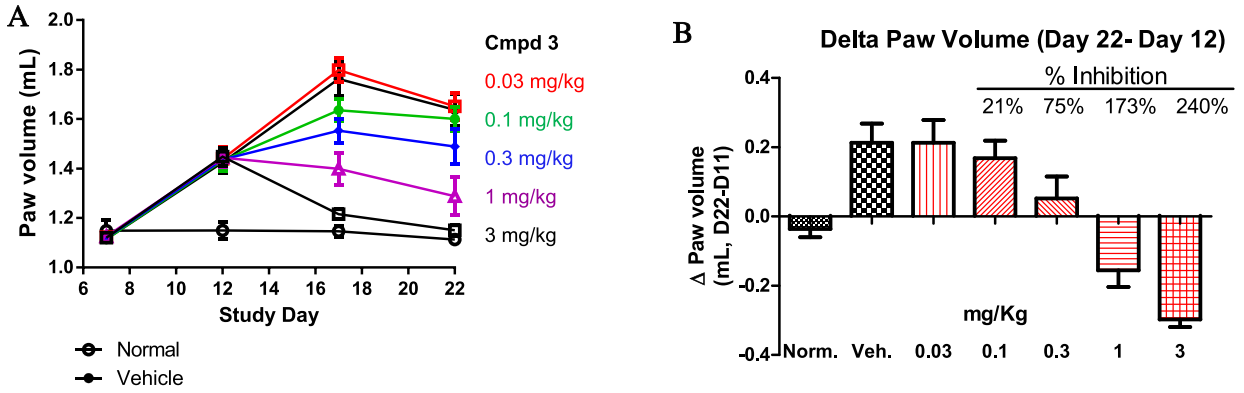

Figure 5. (A) Dose-dependent changes in the paw volume in a rat CIA model at different doses of TAK-020 compound 3 and (B) dose-dependent changes in the paw volume with compound 3 on day 22 of the rat CIA study.

afford a covalent adduct (E-I). In contrast to reversible inhibitors, conventional IC_{50} measurements are of limited value for characterizing the potency of TCIs, nor does measuring the IC_{50} provide a way to evaluate or differentiate similar inhibitors. However, by evaluating both the noncovalent binding to the target (K_i) and the rate at which it reacts with the target nucleophile after reversible binding (k_{inact}), we can obtain valuable information for TCI comparison. We hypothesized that the FBDD principles of efficient ligand growth toward optimal ligand–protein interactions used to arrive at compound 3 would show improved kinetics relative to known covalent Btk inhibitors. To this end, we experimentally evaluated the k_{inact}/K_i ratio in Btk(h) for compound 3 (205×10^6 M^{-1} min^{-1}), Ibrutinib 1 (13×10^6 M^{-1} min^{-1}), CC-292[21] (5×10^6 M^{-1} min^{-1}), and compound 2 (1×10^6 M^{-1} min^{-1}) demonstrating a 16×, 41×, and 205× potency advantage for compound 3 (details in the SI).

Compound 3 Displays PD and Efficacy in a Rat Model of Collagen-Induced Arthritis. In vivo inhibition of phosphorylation of Btk was assessed in a mouse collagen-induced arthritis (CIA) model (Figure 5). After induction of arthritis, compound 3 was dosed at 3, 10, and 30 mg/kg, and % inhibition of pBTK was determined at 2, 4, 8, and 12 h post dosing. Strong inhibition of pBTK was observed at all doses with >50% inhibition remaining at 12 h (Supporting Information). Encouraged by the inhibition of pBTK at these doses, efficacy was investigated in a 22 day rat CIA model. Arthritis was induced in Lewis rats by injecting collagen on day 0 and day 7. By day 11, the disease was established, and compound 3 was administered orally once daily from day 12 to day 21. Compound 3 was dosed QD (once daily) [(0.03, 0.1, 0.3, 1, and 3 mg kg^{-1}) at 24 h intervals] on day 12 of the study and continued through day 21. The paw volume was measured and plotted as the change in the paw volume relative to normal. Compound 3 inhibited paw swelling in a dose-dependent manner with evidence of disease resolution at the highest dose group. When the day 11 paw volume was subtracted from the day 22 paw volume, there was a 240% inhibition of swelling at the top dose 3 mg kg^{-1} with an ED_{50} = 0.17 mg kg^{-1} at an AUC of 4.2 ng h mL^{-1} on day 22 of rat CIA.

Nonclinical Toxicology Safety Evaluation of Compound 3. Compound 3 was subjected to in vitro safety assessment including phototoxicity (negative), phospholipidosis (negative), hERG (acceptable at 18% inhibition at 13 μM), 5-Strain Ames (negative against TA98, TA100, TA1535, TA1537, and WP2 uvrA each with and without S9), micronucleus (negative HPBL with and without S9), UMU genotoxicity (negative), and the Ricerca diversity panel (acceptable PDE3 (96%), PDE5 (67%), and PDE10A2 (59%)). Additionally, 3 was dosed into 2-week rat and 2-week dog dose range-finding toxicology studies after mathematical modeling incorporating PK; targeted occupancy and irreversible enzyme kinetics predicted an efficacious human dose of ~2 mg/day QD.[22] In rat toxicology, 3 was dosed 3, 10, and 75 mg/kg/day with a NOAEL = 10 mg/kg/day, AUC safety multiples of >35× in males/females, ED_{50} AUC in rat CIA (4.2 ng h/mL). In dog toxicology, 3 was dosed 3, 10, and 75 mg/kg/day with a NOAEL = 75 mg/kg/day, AUC safety multiples of 1000×/800× in males/females, ED_{50} AUC in rat CIA (4.2 ng h/mL). There were no target organ toxicities identified in range-finding studies, and the risk was determined as low based on safety exposure multiples.

https://doi.org/10.1021/acs.jmedchem.1c01026
J. Med. Chem. XXXX, XXX, XXX–XXX

CONCLUSIONS

Herein, we describe our strategy to discover an orally available covalent Btk inhibitor with sufficient selectivity over other similar Src and Tek family kinases. Our approach was to start with a highly efficient fragment and incrementally grow it using the tenants of FBDD along with the aid of cocrystal structures, namely, keeping a close watch on the heavy-atom count and lipophilicity constraints (LE and LLE) to rapidly arrive at our lead molecule **3**. The SAR (covered in Table 2) from the initiation of effort until identification of TAK-020 spanned 6 months of synthetic work. The efficiency of TAK-020 and its rapid identification highlighted the advantages of FBDD to the team. Further thorough in vitro and in vivo profiling of **3** followed by CIA models demonstrated both pharmacodynamic (PD) and efficacy endpoints (paw swelling in a rat CIA) being met. Examination of target engagement in vitro and extrapolation toward humans (efficacious dose and target occupancy) revealed that compound **3** could be efficacious at a very low human dose.[22] This led to successful transfer of the program into the clinic; in vivo human PK, PD, and target engagement data have been recently revealed in separate publications.[23]

EXPERIMENTAL SECTION

General Methods for Chemistry. All commercially obtained solvents and reagents were used as received. Microwave-assisted reactions were run in a Biotage initiator. ^{1}H and ^{13}C NMR spectra were recorded on a Bruker Advance 400 or Varian 500. Chemical shifts are reported in parts per million (ppm, δ) using the residual solvent line as a reference. Splitting patterns are designated using the following abbreviations: s, singlet; d, doublet; t, triplet; dd, doublet of doublet; m, multiplet; br, broad. Coupling constants (J) are reported in hertz (Hz). The purity of all final compounds was determined by HPLC, and the compounds are at least ≥95% pure. HPLC purity determination used the following equipment: an Agilent 1200 quaternary pump, an Agilent Autosampler 1200 series, and an Agilent 1200 series DAD. The purity of the test compounds was determined to be ≥95% using one of the following two HPLC conditions. For HPLC method A, a Phenomenex Kinetix C18 column at 200C was used, 2.1 mm × 100 mm, 2.6 μm, eluting with mobile phase A 0.05% TFA in water and mobile phase B 0.0375% TFA in acetonitrile with a flow rate of 1 mL min^{-1} with a gradient of 5−90% B over 6 min. UV detection was performed (λ = 220/254 nm). For HPLC method B, a Phenomenex Kinetix C18 column at 400C was used, 2.1 mm × 100 mm, 2.6 μm, eluting with mobile phase A 0.05% TFA in water and mobile phase B 0.035% TFA in acetonitrile with a flow rate of 1 mL min^{-1} with a gradient of 5−90% B over 6 min. UV detection was performed (λ = 220/254 nm). LC−MS data were acquired on a Waters Acquity UPLC/MS system equipped with a UPLC binary pump, an SQD 3100 mass spectrometer with an electrospray ionization (ESI) source, a PDA detector (210−400 nm), and an evaporative light scattering detector (ELSD). LC was performed using a Waters BEH C18,1.7 μm, ID 2.1 mm × 50 mm at a 55 °C column eluting with mobile phase A 0.05% TFA in water and mobile phase B 0.035% TFA in acetonitrile with a flow rate of 0.8 mL min^{-1} with a gradient of 5−90% B over 1.5 min. The UV absorbance wavelength was sampled at a rate of 20 points s^{-1} between 210 and 400 nm at a resolution of 1.2 nm. High-resolution mass measurements were obtained on a Waters Xevo G2-XS QTof quadrupole time-of-flight mass spectrometer (Waters Corporation, Milford, MA 01757) in positive and negative electrospray modes. The samples were separated using a Waters Acquity UPLC I-Class PLUS system on a BEH 2.1 × 50 mm, 1.7 μm column eluted with mobile phase A 0.01% formic acid in water and mobile phase B methanol, with a flow rate of 0.3 mL min^{-1} with a gradient of 5−90% B over 9.2 min at 60 °C. The mass accuracy was calculated for major observed isotopes against the theoretical mass ions derived from the chemical formula. For experiments described involving animals, all procedures were carried out in compliance with the National Institutes of Health Guide for the Care and Use of Laboratory Animals (1985), under approval of the Institutional Animal Care and Use Committee (IACUC).

Preparation of (*S*)-5-(1-((1-Acryloylpyrrolidin-3-yl)oxy)-isoquinolin-3-yl)-2,4-dihydro-3*H*-1,2,4-triazol-3-one (3). *Step 1: (S)-tert-Butyl 3-((3-chloroisoquinolin-1-yl)oxy)pyrrolidine-1-carboxylate.* To (*S*)-*tert*-butyl 3-hydroxypyrrolidine-1-carboxylate (1.134 g, 6.06 mmol) in NMP (10 mL) at 0 °C was added NaH (60%) (202 mg, 5.05 mmol). The mixture was stirred for 5 min, and 1,3-dichloroisoquinoline (1.000 g, 5.05 mmol) was added. The reaction mixture was stirred at RT for 5 min and then heated at 135 °C for 30 min in a microwave reactor. The mixture was diluted with water (400 mL) and extracted with EtOAc (3 × 125 mL). The organic layers were combined, washed with brine, dried over Na_2SO_4, filtered, and concentrated in vacuo. The crude product was purified by silica column chromatography eluting with a gradient of 25−50% EtOAc in hexane to give the title compound (5.29 g, 75%). ^{1}H NMR (500 MHz, DMSO-d_6): δ 1.40 (d, J = 14.16 Hz, 9 H), 2.12−2.34 (m, 2 H), 3.42−3.58 (m, 3 H), 3.69 (td, J = 12.33, 4.64 Hz, 1 H), 5.63−5.76 (m, 1 H), 7.59 (s, 1 H), 7.64 (ddd, J = 8.30, 7.08, 1.22 Hz, 1 H), 7.81 (td, J = 7.57, 1.46 Hz, 1 H), 7.87−7.92 (m, 1 H), 8.11−8.19 (m, 1 H); ESI-MS m/z: [M + H-*tert*-butyl]$^{+}$, 293.5.

Step 2: (S)-tert-Butyl 3-((3-cyanoisoquinolin-1-yl)oxy)-pyrrolidine-1-carboxylate. A solution of (*S*)-*tert*-butyl 3-((3-chloroisoquinolin-1-yl)oxy)pyrrolidine-1-carboxylate (4.430 g, 12.70 mmol), zinc cyanide (2.980 g, 25.40 mmol), and $Pd(PPh_3)_4$ (1.468 g, 1.27 mmol) in DMF (36.3 mL) was heated at 160 °C for 20 min in a microwave reactor. The reaction mixture was filtered, diluted with water (400 mL), and extracted with EtOAc (2 × 100 mL). The organic layers were combined, washed with brine, dried over Na_2SO_4, and concentrated in vacuo. The crude product was purified by silica column chromatography to give the title compound as a white-to-pale-yellow solid (3.570 g, 83%). ^{1}H NMR (500 MHz, DMSO-d_6): δ 1.40 (d, J = 13.18 Hz, 9 H), 2.23 (d, J = 11.23 Hz, 2 H), 3.42−3.59 (m, 3 H), 3.65−3.75 (m, 1 H), 5.68−5.80 (m, 1 H), 7.82−7.89 (m, 1 H), 7.91−7.98 (m, 1 H), 8.06 (d, J = 8.79 Hz, 1 H), 8.21−8.30 (m, 2 H); ESI-MS m/z: [M + H-*tert*-butyl]$^{+}$, 284.6.

Step 3: (S)-tert-Butyl 3-((3-(5-oxo-4,5-dihydro-1H-1,2,4-triazol-3-yl)isoquinolin-1-yl)oxy)pyrrolidine-1-carboxylate. (*S*)-*tert*-Butyl 3-((3-cyanoisoquinolin-1-yl)oxy)pyrrolidine-1-carboxylate (4.670 g, 13.76 mmol), ethyl hydrazinecarboxylate (7.160 g, 68.80 mmol), DBU (1.037 mL, 6.88 mmol), and NMP (34.6 mL) were mixed in a 200 mL high-pressure reaction vessel. The resulting suspension was heated at 170 °C overnight and was then cooled to room temperature. Crushed ice was added, and the mixture was stirred. A yellow precipitate was collected by vacuum filtration, washed with additional water, and dried in a vacuum oven at 45 °C overnight to give the title compound, which was used in the next step without further purification (5.47 g). ^{1}H NMR (500 MHz, DMSO-d_6): δ 1.33−1.51 (m, 9 H), 2.09−2.38 (m, 2 H), 3.39−3.60 (m, 3 H), 3.75 (dd, J = 12.20, 4.88 Hz, 1 H), 6.03−6.22 (m, 1 H), 7.62−7.71 (m, 1 H), 7.81 (td, J = 7.57, 1.46 Hz, 1 H), 7.95−8.05 (m, 1 H), 8.11−8.29 (m, 2 H), 11.78 (s, 1 H), 12.03 (br s, 1 H).

Step 4: (S)-5-(1-(Pyrrolidin-3-yloxy)isoquinolin-3-yl)-2,4-dihydro-3H-1,2,4-triazol-3-one. To a 200 mL round-bottom flask charged with crude (*S*)-*tert*-butyl 3-((3-(5-oxo-4,5-dihydro-1*H*-1,2,4-triazol-3-yl)isoquinolin-1-yl)oxy)pyrrolidine-1-carboxylate (5.47 g) and dioxane (27.5 mL) was added 4 M HCl in dioxane (13.76 mL, 55.1 mmol). The suspension was stirred at RT with periodic monitoring by HPLC. Upon completion, the reaction mixture was concentrated in vacuo to give a HCl salt of the title compound as a light tan powder that was dried and used without further purification. ESI-MS m/z: [M + H]$^{+}$, 298.6.

Step 5: (S)-5-(1-((1-Acryloylpyrrolidin-3-yl)oxy)isoquinolin-3-yl)-2,4-dihydro-3H-1,2,4-triazol-3-one. To a suspension of (*S*)-5-(1-(pyrrolidin-3-yloxy)isoquinolin-3-yl)-2,4-dihydro-3*H*-1,2,4-triazol-3-onehydrochloride (4.29 g) in DCM (48.1 mL) was added 2,6-dimethylpyridine (3.19 mL, 27.4 mmol). Upon cooling the suspension to 0 °C, acryloyl chloride (1.3 mL, 15.9 mmol) was

https://doi.org/10.1021/acs.jmedchem.1c01026
J. Med. Chem. XXXX, XXX, XXX−XXX

added dropwise. The reaction mixture was stirred for 15 min and warmed to RT over a period of 90 min. Additional 2,6-dimethylpyridine (1.68 mL, 14.43 mmol) and acryloyl chloride (0.469 mL, 5.77 mmol) were added, and the mixture was stirred until HPLC indicated that the reaction was completed. The product was collected by vacuum filtration, washed with DCM, and dried to give the title compound as a pale yellow solid (1.929 g, 39.9% over 3 steps). ^{1}H NMR (400 MHz, DMSO-d_6): δ 2.19−2.48 (m, 2 H), 3.60−4.11 (m, 4 H), 5.63−5.73 (m, 1 H), 6.12−6.23 (m, 2 H), 6.55−6.72 (m, 1 H), 7.66 (tdd, J = 7.64, 7.64, 2.10, 1.19 Hz, 1 H), 7.78−7.84 (m, 1 H), 7.97−8.04 (m, 2 H), 8.17 (d, J = 8.28 Hz, 1 H), 11.79 (s, 1 H), 12.04 (br d, J = 9.66 Hz, 1 H); HRMS: $[M]^+$ calculated for $C_{18}H_{17}N_5O_3$, 351.1331; found, 351.1329.

■ ASSOCIATED CONTENT

Supporting Information

The Supporting Information is available free of charge at https://pubs.acs.org/doi/10.1021/acs.jmedchem.1c01026.

Molecular formula strings for all compounds, synthetic procedures for all analogs not detailed in the main paper, ^{1}H NMR spectra for compounds **3** and **5**−**24**, representative HPLC data for compounds **3**, **5**, and **18** along with ADME and PK experimental procedures, and X-ray cocrystal structure experimental details; methods for determining intrinsic reactivity (nonenzymatic) and bioactivation evaluation of compound **3**, biological evaluation of Btk inhibition, measurement of cellular Btk phosphorylation, in vitro evaluation of potency (k_{inact}/K_i), procedures for conducting the rat collagen-induced arthritis (CIA) model, and the broad kinase inhibition data set for **3** (PDF)

Accession Codes

Compound **5**, 7N5O; compound **6**, 7N5R; compound **18**, 7N5X; compound **3**, 7N5Y. Authors will release the atomic coordinates and experimental data upon article publication. PDB IDs have been provided in figure legends.

■ AUTHOR INFORMATION

Corresponding Author

Mark Sabat − *Takeda California, San Diego, California 92121, United States*; orcid.org/0000-0001-8916-1203; Phone: (+1) 858-205-0419; Email: mark.sabat@takeda.com

Authors

Douglas R Dougan − *Takeda California, San Diego, California 92121, United States*

Beverly Knight − *Pfizer, San Diego, California 92121, United States*

J. David Lawson − *Mirati Therapeutics, Inc., San Diego, California 92121, United States*

Nicholas Scorah − *Takeda California, San Diego, California 92121, United States*

Christopher R Smith − *Mirati Therapeutics, Inc., San Diego, California 92121, United States*

Ewan R Taylor − *Takeda California, San Diego, California 92121, United States*

Phong Vu − *Takeda California, San Diego, California 92121, United States*

Corey Wyrick − *Takeda California, San Diego, California 92121, United States*

Haixia Wang − *Takeda California, San Diego, California 92121, United States*

Deepika Balakrishna − *Takeda California, San Diego, California 92121, United States*

Mark Hixon − *VeriSIM Life, San Francisco, California 94104, United States*

Loui Madakamutil − *Invivoscribe Therapeutics, Inc., San Diego, California 92121, United States*

Donavon McConn − *Takeda California, San Diego, California 92121, United States*

Complete contact information is available at: https://pubs.acs.org/10.1021/acs.jmedchem.1c01026

Author Contributions

The manuscript was written through contributions of all authors. All authors have given approval to the final version of the manuscript.

Notes

The authors declare the following competing financial interest(s): The authors are or were employees of Takeda Pharmaceutical Company. All research described in this manuscript was funded by Takeda Pharmaceutical Company.

■ ACKNOWLEDGMENTS

The staff of the Berkeley Center for Structural Biology is gratefully acknowledged for support of the Beamline 5.0.3 at the Advanced Light Source. The Advanced Light Source is supported by the Director, Office of Science, Office of Basic Energy Sciences, of the U.S. Department of Energy under Contract No. DE-AC02-05CH11231. We acknowledge the contributions of the following Takeda California scientists: Jacques Ermolieff, Petro Halkowycz, Ched Grimshaw, Gavin Hirst, Weston Lane, Michael Klein, Matthew Marx, Lisa Rahbaek, Bi-Ching Sang, Lihong Shi, Gyorgy Snell, Isabelle Tcholakov, Catherine Pham, KimKim Dao, and Haihong Wu.

■ ABBREVIATIONS

Btk, Bruton's tyrosine kinase; Btk-KD, kinase domain of Btk; Cl, clearance; Da, Daltons; E_h, extraction ratio; Jak, Janus kinase; Lck, lymphocyte-specific protein tyrosine kinase; HLM, human liver microsomes; RLM, rat liver microsomes; V_d, volume of distribution

■ REFERENCES

(1) (a) Firestein, G. S. Evolving concepts of rheumatoid arthritis. *Nature* **2003**, *423*, 356−361. (b) Helmick, C. G.; Felson, D. T.; Lawrence, R. C.; Gabriel, S.; Hirsch, R.; Kwoh, C. K.; Liang, M. H.; Kremers, H. M.; Mayes, M. D.; Merkel, P. A.; Pillemer, S. R.; Reveille, J. D.; Stone, J. H.; National Arthritis Data Workgroup. Estimates of the prevalence of arthritis and other rheumatic conditions in the United States: Part I. *Arthritis Rheum.* **2008**, *58*, 15−25. (c) Smolen, J. S.; Aletaha, D. Rheumatoid arthritis therapy reappraisal: strategies, opportunities and challenges. *Nat. Rev. Rheumatol.* **2015**, *11*, 276−289.

(2) (a) Kremer, J. M.; Bloom, B. J.; Breedveld, F. C.; Coombs, J. H.; Fletcher, M. P.; Gruben, D.; Krishnaswami, S.; Burgos-Vargas, R.; Wilkinson, B.; Zerbini, C. A. F.; Zwillich, S. H. The safety and efficacy of a JAK inhibitor in patients with active rheumatoid arthritis: Results of a double-blind, placebo-controlled phase IIa trial of three dosage levels of CP-690,550 versus placebo. *Arthritis Rheum.* **2009**, *60*, 1895−1905. (b) Flanagan, M. E.; Blumenkopf, T. A.; Brissette, W. H.; Brown, M. F.; Casavant, J. M.; Shang-Poa, C.; Doty, J. L.; Elliott, E. A.; Fisher, M. B.; Hines, M.; Kent, C.; Kudlacz, E. M.; Lillie, B. M.; Magnuson, K. S.; McCurdy, S. P.; Munchhof, M. J.; Perry, B. D.; Sawyer, P. S.; Strelevitz, T. J.; Subramanyam, C.; Sun, J.; Whipple, D. A.; Changelian, P. S. Discovery of CP-690,550: a potent and selective

Janus kinase (JAK) inhibitor for the treatment of autoimmune diseases and organ transplant rejection. *J. Med. Chem.* **2010**, *53*, 8468−8484.
(3) Tsukada, S.; Saffran, D. C.; Rawlings, D. J.; Parolini, O.; Allen, R. C.; Klisak, I.; Sparkes, R. S.; Kubagawa, H.; Mohandas, T.; Quan, S.; Belmont, J. W.; Cooper, M. D.; Conley, M. E.; Witte, O. N. Deficient expression of a B cell cytoplasmic tyrosine kinase in human X-linked agammaglobulinemia. *Cell* **1993**, *72*, 279−290.
(4) (a) Kawakami, Y.; Yao, L.; Miura, T.; Tsukada, S.; Witte, O. N.; Kawakami, T. Tyrosine phosphorylation and activation of Bruton tyrosine kinase upon Fc epsilon RI cross-linking. *Mol. Cell. Biol.* **1994**, *14*, 5108−5113. (b) Smith, C. I.; Baskin, B.; Humire-Greiff, P.; Zhou, J. N.; Olsson, P. G.; Maniar, H. S.; Kjellén, P.; Lambris, J. D.; Christensson, B.; Hammarström, L. Expression of Bruton's agammaglobulinemia tyrosine kinase gene, BTK, is selectively down-regulated in T lymphocytes and plasma cells. *J. Immunol.* **1994**, *152*, 557−565.
(5) de Weers, M.; Verschuren, M. C. M.; Kraakman, M. E. M.; Mensink, R. G. J.; Schuurman, R. K. B.; van Dongen, J. J. M.; Hendriks, R. W. The Bruton's tyrosine kinase gene is expressed throughout B cell differentiation, from early precursor B cell stages preceding immunoglobulin gene rearrangement up to mature B cell stages. *Eur. J. Immunol.* **1993**, *23*, 3109−3114.
(6) Lachance, G.; Levasseur, S.; Naccache, P. H. Chemotactic factor-induced recruitment and activation of Tec family kinases in human neutrophils. Implication of phosphatidynositol 3-kinases. *J. Biol. Chem.* **2002**, *277*, 21537−21541.
(7) Gagliardi, M. C.; Finocchi, A.; Orlandi, P.; Cursi, L.; Cancrini, C.; Moschese, V.; Miyawaki, T.; Rossi, P. Bruton's tyrosine kinase defect in dendritic cells from X-linked agammaglobulinaemia patients does not influence their differentiation, maturation and antigen-presenting cell function. *Clin. Exp. Immunol.* **2003**, *133*, 115−122.
(8) (a) Whyatt, D.; Lindeboom, F.; Karis, A.; Ferreira, R.; Milot, E.; Hendriks, R.; de Bruijn, M.; Langeveld, A.; Gribnau, J.; Grosveld, F.; Philipsen, S. An intrinsic but cell-nonautonomous defect in GATA-1-overexpressing mouse erythroid cells. *Nature* **2000**, *406*, 519−524. (b) Robinson, D.; Chen, H.-C.; Li, D.; Yustein, J. T.; He, F.; Lin, W. C.; Hayman, M. J.; Kung, H. J. Tyrosine kinase expression profiles of chicken erythro-progenitor cells and oncogene-transformed erythroblasts. *J. Biomed. Sci.* **1998**, *5*, 93−100.
(9) Quek, L. S.; Bolen, J.; Watson, S. P. A role for Bruton's tyrosine kinase (Btk) in platelet activation by collagen. *Curr. Biol.* **1998**, *8*, 1137−11S1.
(10) Phillips, R. L.; Ernst, R. E.; Brunk, B.; Ivanova, N.; Mahan, M. A.; Deanehan, J. K.; Moore, K. A.; Overton, G. C.; Lemischka, I. R. The genetic program of hematopoietic stem cells. *Science* **2000**, *288*, 1635−1640.
(11) (a) Di Paolo, J. A.; Huang, T.; Balazs, M.; Barbosa, J.; Barck, K. H.; Bravo, B. J.; Carano, R. A. D.; Darrow, J.; Davies, D. R.; DeForge, L. E.; Diehl, L.; Ferrando, R.; Gallion, S. L.; Giannetti, A. M.; Gribling, P.; Hurez, V.; Hymowitz, S. G.; Jones, R.; Kropf, J. E.; Lee, W. P.; Maciejewski, P. M.; Mitchell, S. A.; Rong, H.; Staker, B. L.; Whitney, J. A.; Yeh, S.; Young, W. B.; Yu, C.; Zhang, J.; Reif, K.; Currie, K. S. Specific Btk inhibition suppresses B cell- and myeloid cell-mediated arthritis. *Nat. Chem. Biol.* **2011**, *7*, 41−50. (b) Lou, Y.; Han, X.; Kuglstatter, A.; Kondru, R. K.; Sweeney, Z. K.; Soth, M.; McIntosh, J.; Litman, R.; Suh, J.; Kocer, B.; Davis, D.; Park, J.; Frauchiger, S.; Dewdney, N.; Zecic, H.; Taygerly, J. P.; Sarma, K.; Hong, J.; Hill, R. J.; Gabriel, T.; Goldstein, D. M.; Owens, T. D. Structure-based drug design of RN486, a potent and selective Bruton's tyrosine kinase (BTK) inhibitor, for the treatment of rheumatoid arthritis. *J. Med. Chem.* **2015**, *58*, 512−516. (c) Xu, D.; Kim, Y.; Postelnek, J.; Vu, M. D.; Hu, D.-Q.; Liao, C.; Bradshaw, M.; Hsu, J.; Zhang, J.; Pashine, A.; Srinivasan, D.; Woods, J.; Levin, A.; O'Mahony, A.; Owens, T. D.; Lou, Y.; Hill, R. J.; Narula, S.; DeMartino, J.; Fine, J. S. RN486, a selective Bruton's tyrosine kinase inhibitor, abrogates immune hypersensitivity responses and arthritis in rodents. *J. Pharmacol. Exp. Ther.* **2012**, *341*, 90−103. (d) Liu, L.; Di Paolo, J.; Barbosa, J.; Rong, H.; Reif, K.; Wong, H. Antiarthritis effect of a novel Bruton's tyrosine kinase (BTK) inhibitor in rat collagen-induced arthritis and mechanism-based pharmacokinetic/pharmacodynamic modeling: relationships between inhibition of BTK phosphorylation and efficacy. *J. Pharmacol. Exp. Ther.* **2011**, *338*, 154−163. (e) Kim, K.-H.; Maderna, A.; Schnute, M. E.; Hegen, M.; Mohan, S.; Miyashiro, J.; Lin, L.; Li, E.; Keegan, S.; Lussier, J.; Wrocklage, C.; Nickerson-Nutter, C. L.; Wittwer, A. J.; Soutter, H.; Caspers, N.; Han, S.; Kurumbail, R.; Dunussi-Joannopoulos, K.; Douhan, J., III; Wissner, A. Imidazo[1,5-*a*]quinoxalines as irreversible BTK inhibitors for the treatment of rheumatoid arthritis. *Bioorg. Med. Chem. Lett.* **2011**, *21*, 6258−6263. (f) Chang, B. Y.; Huang, M. M.; Francesco, M.; Chen, J.; Sokolove, J.; Magadala, P.; Robinson, W. H.; Buggy, J. J. The Bruton tyrosine kinase inhibitor PCI-32765 ameliorates autoimmune arthritis by inhibition of multiple effector cells. *Arthritis Res. Ther.* **2011**, *13*, R115. (g) Honigberg, L. A.; Smith, A. M.; Sirisawad, M.; Verner, E.; Loury, D.; Chang, B.; Li, S.; Pan, Z.; Thamm, D. H.; Miller, R. A.; Buggy, J. J. The Bruton tyrosine kinase inhibitor PCI-32765 blocks B-cell activation and is efficacious in models of autoimmune disease and B-cell malignancy. *Proc. Natl. Acad. Sci.* **2010**, *107*, 13075−13080. (h) Shi, Q.; Tebben, A.; Dyckman, A. J.; Li, H.; Liu, C.; Lin, J.; Spergel, S.; Burke, J. R.; McIntyre, K. W.; Olini, G. C.; Strnad, J.; Surti, N.; Muckelbauer, J. K.; Chang, C.; An, Y.; Cheng, L.; Ruan, Q.; Leftheris, K.; Carter, P. H.; Tino, J.; De Lucca, G. V. Purine derivatives as potent Bruton's tyrosine kinase (BTK) inhibitors for autoimmune diseases. *Bioorg. Med. Chem. Lett.* **2014**, *24*, 2206−2211.
(12) (a) Pan, Z.; Scheerens, H.; Li, S.-J.; Schultz, B. E.; Sprengeler, P. A.; Burrill, L. C.; Mendonca, R. V.; Sweeney, M. D.; Scott, K. C. K.; Grothaus, P. G.; Jeffery, D. A.; Spoerke, J. M.; Honigberg, L. A.; Young, P. R.; Dalrymple, S. A.; Palmer, J. T. Discovery of selective irreversible inhibitors for Bruton's tyrosine kinase. *ChemMedChem* **2007**, *2*, 58−61. (b) Wu, J.; Zhang, M.; Liu, D. Acalabrutinib (ACP-196): a selective second-generation BTK inhibitor. *J Hematol. Oncol.* **2016**, *9*, 21−24. (c) Norman, P. Investigational Bruton's tyrosine kinase inhibitors for the treatment of rheumatoid arthritis. *Expert Opin. Invest. Drugs* **2016**, *25*, 891−899.
(13) (a) Twenty-seven diverse fragments were prioritized for X-ray cocrystallography soaking experiments after the first confirmation of binding by a saturated transfer difference. Of these, 20 were successful. We attribute this high success rate to preselecting confirmed binders and to the facile nature of the Btk protein cocrystallography system. The team's noncovalent strategy was disclosed earlier in this journal: (b) Smith, C. R.; Dougan, D. R.; Komandla, M.; Kanouni, T.; Knight, B.; Lawson, J. D.; Sabat, M.; Taylor, E. R.; Vu, P.; Wyrick, C. Fragment-based discovery of a small molecule inhibitor of Bruton's tyrosine kinase. *J. Med. Chem.* **2015**, *58*, 5437−5444.
(14) For a recent review of FBDD, see (a) Kirsch, P.; Hartman, A. M.; Hirsch, A. K. H.; Empting, M. Concepts and core principles of fragment-based drug design. *Molecules* **2019**, *24*, 4309−4330. (b) Hopkins, A. L.; Groom, C. R.; Alex, A. Ligand efficiency: a useful metric for lead selection. *Drug Discovery Today* **2004**, *9*, 430−431. (c) Leeson, P. D.; Springthorpe, B. The influence of drug-like concepts on decision-making in medicinal chemistry. *Nat. Rev. Drug Discovery* **2007**, *6*, 881−890. (d) Hann, M. M.; Keserü, G. M. Finding the sweet spot: the role of nature and nurture in medicinal chemistry. *Nat. Rev. Drug Discovery* **2012**, *11*, 355−365.
(15) Modi, V.; Dunbrack, R. L., Jr. A structurally-validated multiple sequence alignment of 497 human protein kinase domains. *Sci. Rep.* **2019**, *9*, 19790−19804.
(16) (a) Barf, T.; Kaptein, A. Irreversible protein kinase inhibitors: balancing the benefits and risks. *J. Med. Chem.* **2012**, *55*, 6243−6262. (b) Carmi, C.; Cavazzoni, A.; Vezzosi, S.; Bordi, F.; Vacondio, F.; Silva, C.; Rivara, S.; Lodola, A.; Alfieri, R. R.; La Monica, S.; Galetti, M.; Ardizzoni, A.; Petronini, P. G.; Mor, M. Novel irreversible epidermal growth factor receptor inhibitors by chemical modulation of the cysteine-trap portion. *J. Med. Chem.* **2010**, *53*, 2038−2050. (c) Flanagan, M. E.; Abramite, J. A.; Anderson, D. P.; Aulabaugh, A.; Dahal, U. P.; Gilbert, A. M.; Li, C.; Montgomery, J.; Oppenheimer, S.

https://doi.org/10.1021/acs.jmedchem.1c01026
J. Med. Chem. XXXX, XXX, XXX−XXX

R.; Ryder, T.; Schuff, B. P.; Uccello, D. P.; Walker, G. S.; Wu, Y.; Brown, M. F.; Chen, J. M.; Hayward, M. M.; Noe, M. C.; Obach, R. S.; Philippe, L.; Shanmugasundaram, V.; Shapiro, M. J.; Starr, J.; Stroh, J.; Che, Y. Chemical and computational methods for the characterization of covalent reactive groups for the prospective design of irreversible inhibitors. *J. Med. Chem.* **2014**, *57*, 10072−10079. (d) Singh, J.; Petter, R. C.; Baillie, T. A.; Whitty, A. The resurgence of covalent drugs. *Nat. Rev. Drug Discovery* **2011**, *10*, 307−317. (e) Dahal, U. P.; Obach, R. S.; Gilbert, A. M. Benchmarking *in vitro* covalent binding burden as a tool to assess potential toxicity caused by nonspecific covalent binding of covalent drugs. *Chem. Res. Toxicol.* **2013**, *26*, 1739−1745.

(17) Straus, D. B.; Weiss, A. Genetic evidence for the involvement of the lck tyrosine kinase in signal transduction through the T cell antigen receptor. *Cell* **1992**, *70*, 585−593.

(18) (a) Pérez, M. A.; Dorado, C. A.; Soto, J. L. Regioselective synthesis of 1,2,4-triazole and 1,2,4-oxadiazole derivatives. *Synthesis* **1983**, *6*, 483−486. (b) Davoodnia, A.; Bakavoli, M.; Soleimany, M.; Behmadi, H. A new one-pot neat synthesis of 1,2,4-triazol-3-ones through 4-(*N*,*N*-dimethylamino) pyridine (DMAP) catalyzed cyclo-condensation of ethyl carbazate with aryl nitriles. *Chin. Chem. Lett.* **2008**, *19*, 685−688.

(19) Fuchs, A.; Leigh, M.; Kloefer, B.; Dressman, J. B. Advances in the design of fasted state simulating intestinal fluids: FaSSIF-V3. *Eur. J. Pharm. Biopharm.* **2015**, *94*, 229−240.

(20) Irvine, J. D.; Takahashi, L.; Lockhart, K.; Cheong, J.; Tolan, J. W.; Selick, H. E.; Grove, J. R. Mdck (madin-darby canine kidney) cells: A tool for membrane permeability screening. *J. Pharm. Sci.* **1999**, *88*, 28−33.

(21) (a) Brown, J. R.; Harb, W. A.; Hill, B. T.; Gabrilove, J.; Sharman, J. P.; Schreeder, M. T.; Barr, P. M.; Foran, J. M.; Miller, T. P.; Burger, J. A.; Kelly, K. R.; Mahadevan, D.; Ma, S.; Li, Y.; Pierce, D. W.; Barnett, E.; Marine, J.; Miranda, M.; Azaryan, A.; Yu, X.; Nava-Parada, P.; Mei, J.; Kipps, T. J. Phase I study of single-agent CC-292, a highly selective Bruton's tyrosine kinase inhibitor, in relapsed/refractory chronic lymphocytic leukemia. *Haematologica* **2016**, *101*, e295−e298. (b) CC-292 Spebrutinib CAS number 1202757-89-8. (c) Schafer, P. H.; Kivitz, A. J.; Ma, J.; Korish, S.; Sutherland, D.; Li, L.; Azaryan, A.; Kosek, J.; Adams, M.; Capone, L.; Hur, E. M.; Hough, D. R.; Ringheim, G. E. Spebrutinib (CC-292) affects markers of B cell activation, chemotaxis, and osteoclasts in patients with rheumatoid arthritis: Results from a mechanistic study. *Rheumatol Ther.* **2020**, *7*, 101−119. (d) CC-292 also known as AVL-292 and Spebrutinib is commercially available; CAS# 1202757-89-8, MFCD25976876

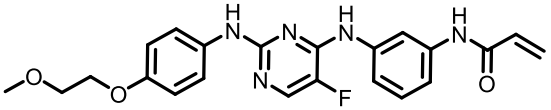

CC-292

(22) For predicting the efficacious human dose and the human pharmacokinetics of TAK-020, a combination of allometric scaling methods, compartmental modeling and physiologically based pharmacokinetic (PBPK) modeling, was employed to simulate the human pharmacokinetics of TAK-020. Efficacious concentrations were based on published data from a clinical BTK inhibitor, CC-292. Evans, E. K.; Tester, R.; Aslanian, S.; Karp, R.; Sheets, M.; Labenski, M. T.; Witowski, S. R.; Lounsbury, H.; Chaturvedi, P.; Mazdiyasni, H.; Zhu, Z.; Nacht, M.; Freed, M. I.; Petter, R. C.; Dubrovskiy, A.; Singh, J.; Westlin, W. F. Inhibition of Btk with CC-292 provides early pharmacodynamic assessment of activity in mice and humans. *J. Pharmacol. Exp. Ther.* **2013**, *346*, 219−228. The initial TAK-020 human dose prediction was designed to approximate the enzyme occupancy achieved by CC-292 at a reported clinically efficacious dose following solution dosing. Additional simulations were performed to approximate a range of target occupancies. The predicted human single-dose solution doses required to achieve ∼10, ∼20, ∼50, ∼85, and ∼99% enzyme occupancy in humans at peak occupancy were 0.05, 0.10, 0.3, 1.0, and 4.0 mg, respectively.

(23) Esfandiari, E.; Chen, M.; Smithson, G.; Blair, D.; Faessel, H.; Wagner, J.; Mclean, L.; Fedyk, E. R. A phase I, randomized, double-blind, placebo-controlled, single-dose and multiple-rising-dose study of the BTK inhibitor TAK-020 in healthy subjects. *Clin. Transl. Sci.* **2021**, 820.

https://doi.org/10.1021/acs.jmedchem.1c01026
J. Med. Chem. XXXX, XXX, XXX−XXX